Singular tori as attractors of four-wave-interaction systems

S. Lagrange, D. Sugny,[*] A. Picozzi, and H. R. Jauslin

Laboratoire Interdisciplinaire Carnot de Bourgogne (ICB), UMR 5209, CNRS–Université de Bourgogne, 9 Av. A. Savary,
BP 47 870, F-21078 Dijon Cedex, France
(Received 24 June 2009; published 7 January 2010)

We study the spatiotemporal dynamics of the Hamiltonian four-wave interaction in its counterpropagating configuration. The numerical simulations reveal that, under rather general conditions, the four-wave system exhibits a relaxation process toward a stationary state. Considering the Hamiltonian system associated to the stationary state, we provide a global geometrical view of all the stationary solutions of the system. The analysis reveals that the stationary state converges exponentially toward a pinched torus of the Hamiltonian system in the limit of an infinite nonlinear medium. The singular torus thus plays the role of an *attractor* for the spatiotemporal wave system. The topological properties of the singular torus confer a robust character to the stationary solution when the boundary conditions or the length of the nonlinear medium are modified. Furthermore, an adiabatic approach of the boundary conditions reveals that singular tori also play a major role for the description of the spatiotemporal dynamics of the wave system.

I. INTRODUCTION

Resonant four-wave interaction is ubiquitous in nonlinear science [1] and is found to play a key role in such diverse fields as plasma physics [2], acoustics [3], hydrodynamics [4], and nonlinear optics [5]. More recently, four-wave mixing processes have stimulated particular interest in the study of atomic Bose-Einstein condensates [6], as well as spinor Bose-Einstein condensates, i.e., condensates of atoms with different spins [7]. In this framework, a remarkable example of the importance of four-wave interactions is the coherent matter wave amplification obtained through four-wave interactions involving a pair of light waves and a pair of matter waves [8].

In the context of nonlinear optics, the four-wave interaction has been investigated in various configurations [5]. In particular the dynamics of the polarization of optical beams has been studied in the counterpropagative configuration of the four-wave interaction, in which two beams composed of two polarization states are injected at opposite ends of a nonlinear medium, such as, e.g., an optical fiber [9]. Different studies have shown the richness of this kind of system which can exhibit polarization bistability [10], temporal instabilities [11,12], and solitons [13,14]. More recently, a new effect concerning the polarization dynamics has been studied both numerically and experimentally [15].

The dynamics of the four-wave interaction is governed by a system of four partial differential equations (PDE) that exhibits a Hamiltonian structure with infinitely many degrees of freedom. The complexity of the dynamics is in large part due to the existence of resonant terms coupling the four equations. The originality of this system relies on the boundary conditions which are imposed to the fields at both ends of the nonlinear medium. Under rather general conditions, one may observe a relaxation process of the PDE system toward a stationary state. It is this asymptotic dynamics which re-

veals the geometry of the problem and makes the link with finite-dimensional dynamical systems, i.e., with ordinary differential equations (ODE). Our aim in this work is to exploit recently developed mathematical techniques of Hamiltonian ODE's systems to analyze the dynamics of the spatiotemporal (PDE) four-wave interaction.

Hamiltonian integrable ODE systems have a long and fruitful history extending from Liouville in the mid 19th century to Arnold at the end of the 20th century [16]. An integrable Hamiltonian system with N degrees of freedom has a set of N functions $\{F_1, \cdots, F_N\}$ defined on the $2N$-dimensional phase space of the system which are independent and in involution, i.e., the Poisson bracket of any two functions F_i and F_j vanishes. We also introduce the energy-momentum map $\mathcal{F}$ which sends the points of the initial phase space to a subset of $\mathbb{R}^N$ corresponding to the possible values of the functions $F_1, \ldots, F_N$. Using the Liouville-Arnold theorem under suitable conditions, it can be shown that the preimage of a regular value of $\mathcal{F}$ (a regular value is a value such that the differentials of F_i are linearly independent) is an N-dimensional torus [16]. This also means that $\mathcal{F}$ defines a torus bundle with base space the image of $\mathcal{F}$ and with generic fiber a torus. However, all points of the image of $\mathcal{F}$ are not regular, i.e., they are critical points of $\mathcal{F}$. In this case, the preimage of these points is a critical fiber which can be of different types: a point (for an equilibrium), a circle (for a periodic orbit) or a singular torus. A singular torus is by definition a critical fiber of the torus bundle with singularities as, for instance, a pinched torus. A pinched torus is a singular torus where one of the generating circles shrinks to a point. We refer the reader to Refs. [17–19] for a detailed discussion of singular tori. In this paper, we will show that the Hamiltonian system associated to the four-wave interaction exhibits zero, one or two pinched tori depending on the powers of the two counterpropagating waves. The pinched torus is the unique singular torus encountered in this system.

The importance of singular tori in the dynamics of Hamiltonian systems has been the subject of a growing interest in recent years [17,18]. Singular tori play a major role in the notion of Hamiltonian monodromy introduced by Duister-

_____
[*]dominique.sugny@u-bourgogne.fr

maat in 1980 [21] to answer the important question regarding the extension of local action-angle variables to the whole phase space. Duistermaat showed that a Hamiltonian system with a pinched torus has a non trivial monodromy which is a topological obstruction to the existence of global action-angle variables. Different examples of physical systems with non trivial monodromy have been discovered after this work, both in classical and quantum systems with two or three degrees of freedom [20,22–25].

In a recent letter [26], we have pointed out that singular tori may play a central role in the spatiotemporal dynamics of nonlinear wave systems. Indeed, the PDE system exhibits a relaxation process toward a stationary state which lies in the neighborhood of the singular torus associated to the corresponding ODE system. The present paper is devoted to giving a deeper insight into the role of singular tori in the spatiotemporal four-wave interaction. Exploiting the mathematical techniques developed for Hamiltonian integrable systems [17,18], we determine the position and the nature of singular tori, which are shown to depend crucially on the powers of the two counterpropagating waves. The numerical simulations show that the relaxation process occurs when single or doubly pinched tori exist. The properties of the corresponding stationary state can be deduced from the topology of the singular torus. The singular torus thus plays the role of an *attractor* for the four-wave system, which is an infinite dimensional Hamiltonian system.

The peculiar topological properties of the system having a pinched torus confer a robust character to the stationary solution when the boundary conditions or the length of the nonlinear medium are modified. We develop an adiabatic treatment of the boundary conditions by adapting the adiabatic theory formulated in classical and quantum mechanics [16] to the spatiotemporal wave system considered here. This reveals that *singular tori play a major role not only for the determination of the stationary solutions, but also for the description of the spatiotemporal dynamics*. The adiabatic approach consists in slowly modifying the boundary conditions, i.e., the intensity of the two fields at both ends of the fiber, from 0 to some final stationary value. The position of the singular pinched tori changes following the variations of the boundary conditions. We show that, in the adiabatic limit, the system follows an *instantaneous stationary state* that lies on the corresponding *instantaneous singular torus*. In this way, we calculate the temporal evolution of the position of the singular torus in phase space, which allows us to deduce the whole spatiotemporal dynamics of the four-wave system.

The paper is organized as follows. In Sec. II, we recall the equations governing the counterpropagating four-wave interaction, in which we make use of the formalism of the Stokes vectors to simplify the description of the dynamics. The phase space of the stationary states is the product of two spheres, $S^2 \times S^2$. We formulate some conjectures on the spatiotemporal dynamics, which will be shown to be supported by the numerical simulations of the PDE system. Section III is devoted to a geometrical description of the stationary states. Using singular reduction theory, we determine the nature of the critical fibers of the stationary Hamiltonian system. We show that the existence of singular pinched tori crucially depends on the powers of the counterpropagating

waves. In Sec. IV we present the adiabatic treatment of the boundary conditions, as well as the numerical simulations of the PDE system, which confirm the adiabatic theory and the key role of singular tori in the spatiotemporal dynamics of the four-wave interaction. Some conclusions and discussions are presented in Sec. V.

II. COUNTERPROPAGATING FOUR WAVE INTERACTION

A. Model equations

We consider the one dimensional counterpropagating configuration of the four- wave interaction. For concreteness, we consider the example of an optical fiber system that has been widely studied experimentally [10–12]. The PDEs governing the evolution of the slowly varying envelopes of the forward signal wave and backward pump wave in the circular polarization basis read [9,13–15]

$$\frac{\partial u}{\partial t} + \frac{\partial u}{\partial z} = i[(|u|^2 + 2|v|^2 + 2|\bar{u}|^2 + 2|\bar{v}|^2)u + 2\bar{u}\bar{v}^*v],$$

$$\frac{\partial v}{\partial t} + \frac{\partial v}{\partial z} = i[(|v|^2 + 2|u|^2 + 2|\bar{u}|^2 + 2|\bar{v}|^2)v + 2\bar{u}^*\bar{v}u],$$

$$\frac{\partial \bar{u}}{\partial t} - \frac{\partial \bar{u}}{\partial z} = i[(|\bar{u}|^2 + 2|\bar{v}|^2 + 2|u|^2 + 2|v|^2)\bar{u} + 2uv^*\bar{v}],$$

$$\frac{\partial \bar{v}}{\partial t} - \frac{\partial \bar{v}}{\partial z} = i[(|\bar{v}|^2 + 2|\bar{u}|^2 + 2|u|^2 + 2|v|^2)\bar{v} + 2u^*v\bar{u}]. \quad (1)$$

The fields u and v ($\bar{u}$ and $\bar{v}$) denote the amplitudes of the left and right circular polarization components of the forward (backward) wave. For convenience, we normalized the problem with respect to the characteristic nonlinear interaction time $\tau_0 = 1/(\Gamma e_0^2)$ and length $\Lambda_0 = v\tau_0$, where $\Gamma = 2\gamma/3$, γ being the nonlinear Kerr coefficient of the optical fiber. $v = c/n$ denotes the velocity of the optical fields, c being the speed of light in vacuum and n the refractive index. e_0^2 is the power of the backward pump wave injected at $z=L$. The variables can be recovered in real units through the substitutions $t \to t\tau_0$; $z \to z\Lambda_0$ and $(u,v) \to (u,v)e_0$ [$(\bar{u},\bar{v}) \to (\bar{u},\bar{v})e_0$]. The last term of the right-hand side is a resonant term coupling the circular polarization components of the waves. These terms play a key role in the polarization dynamics described below.

This system is governed by Hamiltonian field equations that can be derived from the following Hamiltonian functional $\mathcal{H} = \int h dz$. The Hamiltonian density $h = h_{nl}^{nr} + h_{nl}^r + h_l$ has a nonresonant nonlinear contribution $h_{nl}^{nr} = -2(|uv|^2 + |u\bar{u}|^2 + |u\bar{v}|^2 + |\bar{u}\bar{v}|^2 + |\bar{v}v|^2 + |\bar{u}v|^2) + \frac{1}{2}(|u|^4 + |v|^4 + |\bar{v}|^4 + |\bar{u}|^4)$, a resonant nonlinear contribution $h_{nl}^r = -2u^*\bar{u}v\bar{v}^* + $c.c., and a linear contribution $h_l = -\frac{i}{2}u^*\partial_z u - \frac{i}{2}v^*\partial_z v + \frac{i}{2}\bar{u}^*\partial_z\bar{u} + \frac{i}{2}\bar{v}^*\partial_z\bar{v} + $c.c., c.c. denoting the complex conjugate. The field variables $(u,v,\bar{u},\bar{v})$ are in $\mathbb{C}^2 \times \mathbb{C}^2$, which is a real eight-dimensional manifold.

The formalism of Stokes vectors is equivalent to the preceding representation up to a global phase factor for the two
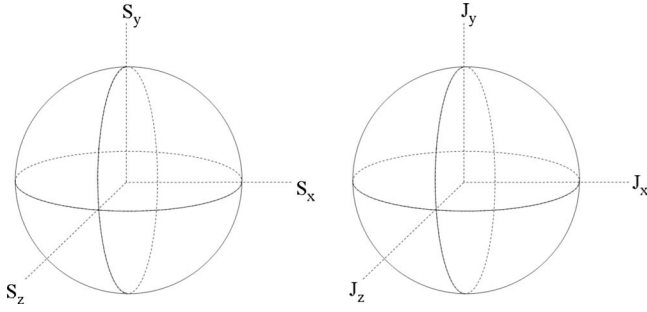
FIG. 1. Phase space $\mathcal{M} = \mathbb{S}^2 \times \mathbb{S}^2$.

waves, whose advantage is to reduce the real dimension to 6. The Stokes vectors $S = (S_x, S_y, S_z)$ and $J = (J_x, J_y, J_z)$ are defined by

$$\begin{cases} S_x = i(u^*v - uv^*) \\ S_y = |u|^2 - |v|^2 \\ S_z = u^*v + uv^* \end{cases} ; \quad \begin{cases} J_x = i(\bar{u}^*\bar{v} - \bar{u}\bar{v}^*) \\ J_y = |\bar{u}|^2 - |\bar{v}|^2 \\ J_z = \bar{u}^*\bar{v} + \bar{u}\bar{v}^* \end{cases} .$$

Within the normalized units, the radius of the backward pump sphere is $J_0^2 = |\vec{J}|^2 = |\bar{u}|^2 + |\bar{v}|^2 \equiv 1$, while the radius of the signal sphere $S_0^2 = |\vec{S}|^2 = |u|^2 + |v|^2$ corresponds to the ratio of the signal and pump powers. For fixed boundary conditions, note that J_0^2 and S_0^2 are conserved during the propagation of the waves. In this representation, the phase space is the product of two spheres, $\mathcal{M} = \mathbb{S}^2 \times \mathbb{S}^2$ as illustrated in Fig. 1. The polarization of each wave is now represented by a point on a sphere. For instance, circular polarization states correspond to the poles of the sphere, whereas linear polarization states correspond to the equator of the sphere [9]. Algebraic manipulations lead to the following spatiotemporal equations satisfied by $\vec{S}$ and $\vec{J}$:

$$\frac{\partial \vec{S}}{\partial t} + \frac{\partial \vec{S}}{\partial z} = \vec{S} \times (\mathcal{J}\vec{S}) + 2\vec{S} \times (\mathcal{J}\vec{J}),$$

$$\frac{\partial \vec{J}}{\partial t} - \frac{\partial \vec{S}}{\partial z} = \vec{J} \times (\mathcal{J}\vec{J}) + 2\vec{J} \times (\mathcal{J}\vec{S}), \quad (2)$$

where $\mathcal{J}$ denotes the diagonal matrix diag$(-1, 0, -1)$.

B. Conjectures on the dynamics

We propose in this section different conjectures describing the asymptotic dynamics of the system in the limit $t \to +\infty$. These conjectures are supported by the numerical integration of the PDE system [Eq. (2)], a feature that will be discussed in detail in Sec. IV. The PDE system [Eq. (2)] is solved numerically with boundary conditions imposed at both ends of the nonlinear medium of length L. The forward field is given at $z=0$, $\vec{S}(z=0, t) = \vec{S}_f$ while the backward field is given at $z=L$, $\vec{J}(z=L, t) = \vec{J}_f$. However, when an optical field enters the nonlinear medium, its amplitude does not reach instantaneously the corresponding stationary value. One should thus consider a boundary condition that varies progressively from 0 to its stationary value. More precisely,

the two waves are subjected to the following boundary conditions $\vec{S}(0, t) = f_1(t)\vec{S}_f$ and $\vec{J}(L, t) = f_2(t)\vec{J}_f$ where f_1 and f_2 are two smooth monotonic functions that evolve from 0 to 1 in a finite but large normalized time τ, $f_{1,2}(0) = 0$ and $f_{1,2}(\tau) = 1$ (see Sec. IV for a concrete example of $f_{1,2}$). Note that the numerical simulations reveal that a sufficient condition to avoid the emergence of instabilities is that the derivative of the function f is continuous, i.e., the function f is $\mathcal{C}^1$.

The two conjectures on the dynamics can be stated as follows:

Conjecture 1. The PDE system [Eq. (2)] relaxes to a stationary solution for each choice of the boundary conditions imposed at both ends of the medium of length L.

Conjecture 2. The stationary solution lies in a singular pinched torus in the limit where the length of the medium goes to infinity ($L \to +\infty$).

Let us underline that the relaxation process toward the stationary state does not take place when the resonant terms are removed in Eqs. (1). This conclusion is consistent with our theory, since in the absence of resonant terms, the system does not exhibit singular tori. We shall see in Sec. IV that these conjectures are supported by the numerical simulations of the PDE system [Eq. (2)]. In the next section we shall describe the geometry of the stationary states. This analysis will allow us to determine the existence, the position and the nature of the singular tori.

III. GEOMETRICAL ANALYSIS OF STATIONARY STATES

We analyze in this section the geometrical structure of the stationary solutions of the PDE system [Eq. (2)]. These solutions satisfy the following system of equations,

$$\frac{\partial \vec{S}}{\partial z} = \vec{S} \times (\mathcal{J}\vec{S}) + 2\vec{S} \times (\mathcal{J}\vec{J}),$$

$$-\frac{\partial \vec{J}}{\partial z} = \vec{J} \times (\mathcal{J}\vec{J}) + 2\vec{J} \times (\mathcal{J}\vec{S}) \quad (3)$$

obtained from the preceding system [Eq. (2)] by dropping the time derivatives. This system can be viewed as a Hamiltonian system on $\mathbb{S}^2 \times \mathbb{S}^2$ where the *coordinate z* plays the role of time. The Hamiltonian H associated to this system can be written as

$$H = 2(S_x J_x + S_z J_z) - \frac{1}{2}(S_y^2 + J_y^2).$$

The two-degree of freedom system with Hamiltonian H is Liouville integrable [16] since it Poisson-commutes with $K = S_y + J_y$. The integrability of this system is due to its axial symmetry with respect to rotations around the z axis [25].

Let us briefly note that the boundary conditions considered here, namely $\vec{S}$ fixed at $z=0$ and $\vec{J}$ fixed at $z=L$, are quite nontrivial from the general perspective of Hamiltonian systems. Indeed, in the traditional temporal language of Hamiltonian (mechanical) systems, the above boundary conditions mean that the state of the system is partially fixed at two different "times:" one variable is fixed at $z=0$, while the

other variable is fixed at a later time $z=L$. It is the specificity of these boundary conditions inherent to the counterpropagating configuration of the wave system that makes the relaxation dynamics possible. In particular, the relaxation process considered in this work is not expected to occur in the copropagating configuration of the four-wave interaction.

A. Bifurcation diagram

We introduce the energy-momentum map $\mathcal{F}$ defined as

$$\mathcal{F}:(\vec{S},\vec{J}) \in \mathbb{S}^2 \times \mathbb{S}^2 \mapsto (H,K) \in \mathbb{R}^2.$$

The object of interest for our study is the image of the energy-momentum map $\mathcal{F}$ which is usually called bifurcation diagram. The analysis of its inverse $\mathcal{F}^{-1}$ and of its critical points will give us a global geometrical view of the different stationary states [17]. A regular value is a point ($H=h$, $K=k$) such that the 1-forms dH or dK are linearly independent at all points of $\mathcal{F}^{-1}(h,k)$. Saying that the 1-forms are linearly dependent is equivalent to say that the rank of the Jacobian matrix of H and K is equal to 2. The Liouville-Arnold theorem states under an hypothesis of compactness and connectedness [16] that $\mathcal{F}^{-1}(h,k)$ is diffeomorphic to a 2-torus. At a critical point where dH and dK are linearly dependent, $\mathcal{F}^{-1}(h,k)$ is a critical fiber, which can be of different types, such as, e.g., a point (for a fixed point), a circle (for a periodic orbit) or a singular torus (a pinched torus). Expressing the 1-forms dH and dK in the basis $(d\vec{S},d\vec{J})$ and taking into account the constraints $|\vec{S}|^2=S_0^2$ and $|\vec{J}|^2=J_0^2$, one deduces that a point of the bifurcation diagram is critical if there exist $(\alpha,\beta,\gamma) \in \mathbb{R}^3 \backslash \{0\}$ such that

$$dH = \alpha dK + \beta dS + \gamma dJ.$$

This condition can be written as

$$\begin{cases} J_x(1-\beta\gamma)=0 \\ J_y(1-\beta\gamma)=0 \\ S_x(1-\beta\gamma)=0 \\ S_y(1-\beta\gamma)=0 \\ J_z=-\alpha/(1+2\gamma) \\ S_z=-\alpha/(1+2\gamma). \end{cases} \quad (4)$$

This system has two different types of solutions:

(i) $1-\beta\gamma=0$: The corresponding solutions are associated to points of the boundary of the image of the energy-momentum map. The preimages of such points are circles.

(ii) $1-\beta\gamma\neq0$: There exist four critical points corresponding to $k=\pm J_0 \pm S_0$ and $h=-(J_0^2+S_0^2)/2$. Two of these points belong to the boundary of the diagram and the corresponding fibers are reduced to simple points. The other two either belong to the boundary or to the interior of the diagram depending on the values of the powers of the waves. When the two powers are equal ($J_0=S_0=1$), the two points coincide, and the corresponding singular torus is doubly pinched.

The different types of bifurcation diagram that can be obtained are represented in Fig. 3. In Fig. 3(a) and 3(b), there exist two interior critical points which are degenerate in (a) and distinct in (b). We shall now determine the topology of the different critical fibers.

B. Reduced phase space and singular tori

We present in this section a complete analysis to determine the geometry of critical fibers. We use different tools based on recent mathematical techniques developed for Hamiltonian integrable systems [17,18]. Since these techniques are relatively new in the physics literature and, in particular in nonlinear optics, we detail below the different steps of the method and we explain qualitatively the different concepts introduced.

Most examples of integrable Hamiltonians with pinched tori are constructed from the momentum $K=(p_1^2+q_1^2-p_2^2-q_2^2)/2$ where (p_1,q_1) and (p_2,q_2) are canonically conjugated coordinates. Hamiltonian systems with this momentum K are called $1:-1$ resonant system since K is the sum of two harmonic oscillators of frequencies $+1$ and -1. The spherical pendulum which has one pinched torus is an example of a locally $1:-1$ resonant system [17].

The main tool used in this section is the reduced phase space. The idea of this approach is to reduce the dimensionality of the problem by using the flow ϕ_K of K [17,18]. To construct this space, one has to determine all the functions which Poisson-commute with K, i.e., in practice a basis of this algebra of functions. This can be done straightforwardly if K is a polynomial and if no constraint is imposed to the system [18]. This is the case for a $1:-1$ resonant system. In our case, the difficulty resides on the peculiar geometry of the phase space, which is a direct product of two spheres $\mathbb{S}^2 \times \mathbb{S}^2$. The construction of the reduced phase space has to be adapted to the constraints due to this geometry. We use for that the results of [25], which deals with a similar mathematical problem, the quantum and classical dynamics of two coupled angular momenta. More precisely, it can be shown that all the polynomial functions which Poisson-commute with K are polynomials in the following four variables Π_j [25]:

$$\begin{cases} \Pi_0 = K = S_y + J_y \\ \Pi_1 = S_y - J_y \\ \Pi_2 = \vec{J} \cdot \vec{S} \\ \Pi_3 = S_z J_x - S_x J_z. \end{cases} \quad (5)$$

These functions fulfill the following relation:

$$\Pi_3^2 + \left[\Pi_2 - \frac{1}{4}(\Pi_0^2 - \Pi_1^2)\right]^2 - \left[S_0^2 - \frac{1}{4}(\Pi_0 + \Pi_1)^2\right]$$
$$\times \left[J_0^2 - \frac{1}{4}(\Pi_0 - \Pi_1)^2\right] = 0, \quad (6)$$

with the constraint $-S_0-J_0 \leq \Pi_0 \leq S_0+J_0$. Using $\{\Pi_i\}$ as new coordinates, the Hamiltonian H can be written as follows:

$$H = 2\Pi_2 - \frac{3}{4}\Pi_0^2 + \frac{1}{4}\Pi_1^2. \quad (7)$$

The reduced phase space $M_{K=k}$ is defined geometrically by

$$M_{K=k} = K^{-1}(k)/S^1, \quad (8)$$

i.e., it is the quotient of the initial phase space by the action of the Hamiltonian flow generated by K. In other words,
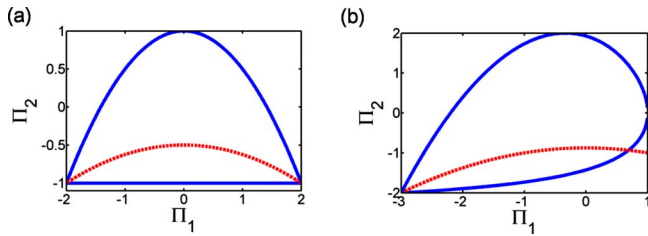
FIG. 2. (Color online) Projection in the space $(\Pi_1, \Pi_2, \Pi_3 = 0)$ of the reduced phase space (solid line in blue) and of the surface $H = h$ (dashed line in red) for (a) identical powers $(J_0 = S_0 = 1)$ and for (b) different powers $(S_0 = J_0/2 = 1/2)$.

$M_{K=k}$ can be thought of as follows: we associate to each periodic orbit defined by the flow ϕ_K and a point of the initial phase space, a point of the reduced phase space. An algebraic construction of this phase space is given using the invariant polynomials (K, Π_1, Π_2, Π_3). For a given value of K, the reduced phase space is defined in the space $\mathbb{R}^3 = (\Pi_1, \Pi_2, \Pi_3)$ by the relation (6), i.e., it corresponds to the surface of the semialgebraic variety defined by Eq. (6) in $\mathbb{R}^3$ [17,18]. Here, due to the reflexion symmetry $\Pi_3 \leftrightarrow -\Pi_3$ with respect to the plane $\Pi_3 = 0$, one can represent the semialgebraic variety $M_{K=k}$ by its projection on the plane $(\Pi_3 = 0)$. This is illustrated in Fig. 2 for equal [case (a)] and different powers [case (b)]. It should be noted that the process used here to construct the reduced phase space is a singular reduction because one or two points (depending on the powers of the waves) do not lift to a circle S^1 in the initial phase space but to a point [17]. To illustrate this remark, we consider the action of ϕ_K which corresponds to a simultaneous rotation around the z axis on the two spheres of the phase space. The north and south poles are invariant by this action. It is then straightforward to see that a point of the phase space associated to two poles (there are four singular points of this kind) does not lift to a circle but to a point since it remains fixed under the action of ϕ_K. Such points are associated to nonsmooth points of the reduced phase space. One sees in Fig. 2 that there are one or two nonsmooth points depending on the values of the powers.

We now analyze the different kinds of critical fibers of the bifurcation diagram. For that purpose, we determine the intersection of the surface $h = H(K = k, \Pi_1, \Pi_2, \Pi_3)$ and of the reduced phase space. Two examples are displayed in Fig. 2 in the plane $\Pi_3 = 0$. Figure 2 displays the lines of equation $h = H(K = k, \Pi_1, \Pi_2, \Pi_3 = 0)$ in the plane (Π_1, Π_2). In our example, the intersection between the two surfaces can be of different types: empty, a point and a circle. An empty intersection corresponds to a point belonging to a forbidden part of the bifurcation diagram, i.e., to a value of (h, k) that is not in the image of $\mathcal{F}$. If the intersection is a smooth point of $M_{K=k}$ then this point lifts to a circle, whereas it lifts to a point if the point is nonsmooth. If the intersection is a circle of smooth points then since each point of the circle lifts to a circle, we get a regular torus. If one or two points of the circle are nonsmooth points of $M_{K=k}$ then one obtains a single or a doubly pinched torus since these points lift to a point in the initial phase space. From a practical point of view, these singular values can be determined by a visual
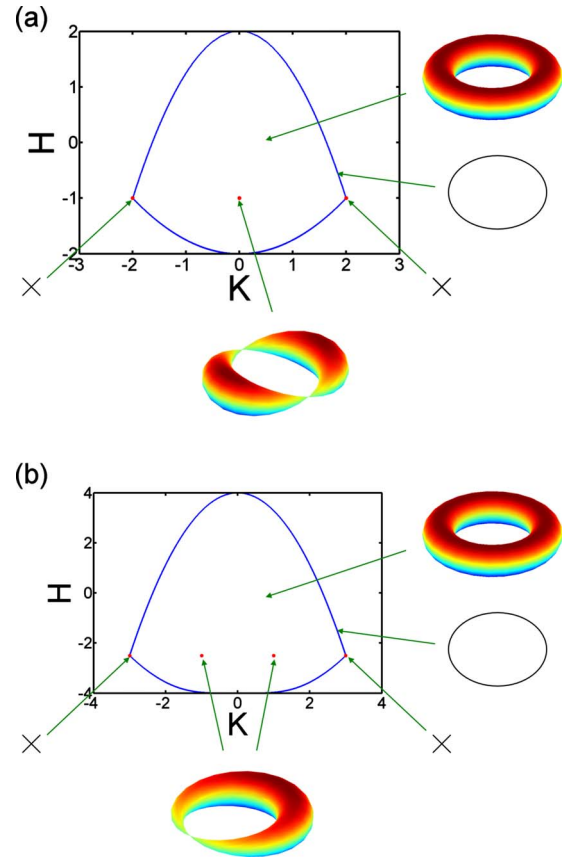
FIG. 3. (Color online) Bifurcation diagram with the critical fibers (single and doubly pinched tori, circle, point) associated to critical points for (a) identical powers and for (b) different powers.

inspection of Fig. 2 by varying h and k. The different kinds of tori are summarized for identical and different powers of the waves in Fig. 3.

C. Boundary conditions and stationary states

1. Methodology

Having shown how to determine the nature and the position of singular tori, we pursue in this section our analysis of the stationary states. Assuming that the values of the boundary conditions are fixed, our aim consists in finding all the stationary solutions of the PDE system [Eq. (2)] compatible with such boundary conditions. To simplify the calculations, we introduce the following canonically conjugate coordinates (I^s, ϕ^s) and (I^p, ϕ^p)

$$\begin{cases} S_x = \sqrt{S_0^2 - I^{s2}} \cos \phi^s \\ S_y = I^s \\ S_z = \sqrt{S_0^2 - I^{s2}} \sin \phi^s \end{cases} ; \quad \begin{cases} J_x = \sqrt{J_0^2 - I^{p2}} \cos \phi^p \\ J_y = I^p \\ J_z = \sqrt{J_0^2 - I^{p2}} \sin \phi^p \end{cases}$$

whose corresponding phase space is a product of two cylinders [13]. Note that these polar coordinates are only defined if $|I^s| < S_0$ and $|I^p| < J_0$, and they are singular at the north and south poles. The Hamiltonian H of the stationary Eqs. (3) can then be written as

$$H = c(I^s, K)\cos(\alpha) - d(I^s, K), \tag{9}$$

where the functions c and d are defined by

$$c(I^s, K) = 2[J_0^2 - (K - I^s)^2]^{1/2}[S_0^2 - I^{s2}]^{1/2}, \tag{10a}$$

$$d(I^s, K) = \frac{1}{2}[I^{s2} + (K - I^s)^2], \tag{10b}$$

and

$$\alpha = \phi^s - \phi^p. \tag{11}$$

K is the constant of the motion, which is given e.g., by

$$K = I^s(L) + I^p(L). \tag{12}$$

In these coordinates, the boundary conditions are expressed by

$$I^p(L) = I_L^p,$$

$$I^s(0) = I_0^s,$$

$$\phi^p(L) = \phi_L^p,$$

$$\phi^s(0) = \phi_0^s. \tag{13}$$

One sees that the value of K and of $\alpha_0 = \alpha(0)$ are not determined explicitly by the conditions (13) since the boundary conditions are specified at different points of the nonlinear medium. The idea is therefore to invert the problem and to interpret K and α_0 as parameters. This means that for given boundary conditions I_0^s et I_L^p and for a given length of the medium L, we determine numerically all possible values of K and α_0, in such a way that the functions f and g

$$I^s(z) = f(z, I_0^s, K, \alpha_0), \tag{14a}$$

$$\alpha(z) = g(z, I_0^s, K, \alpha_0), \tag{14b}$$

correspond to solutions of the Hamiltonian equations. The boundary conditions for the stationary solution $I^s(z)$ can be expressed as

$$I^s(L) = f(L, I_0^s, [I^s(L) + I_L^p], \alpha_0). \tag{15}$$

If there exists at least one couple (K, α_0) compatible with the boundary conditions, i.e., satisfying the relation (15), then for a given value of ϕ_0^s, $\phi^p(0)$ is determined by

$$\phi^p(0) = \phi_0^s - \alpha_0. \tag{16}$$

The angles ϕ_L^p and $\phi^s(L)$ are then computed by solving the Hamiltonian equations.

Using Eq. (12), the relation (15) can be written as

$$I_L^p - K = f(L, I_0^s, [I^s(L) + I_L^p], \alpha_0). \tag{17}$$

The condition (15) is therefore equivalent to the determination of zeros of the function

$$G(K, \alpha_0) = f(L, I_0^s, I^s(L) + I_L^p, \alpha_0) - (I_L^p - K) = 0. \tag{18}$$

We solve numerically Eq. (18) by determining the zeros of G in the plane (K, α_0). Note that the possible values of the
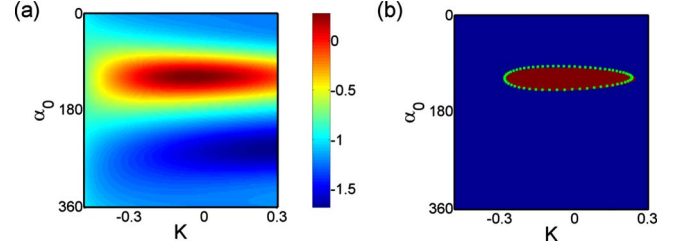
FIG. 4. (Color online) (a) Values of the function $G(K, \alpha_0)$ for the boundary conditions $I_0^s = 0.5$ and $I_L^p = -0.71$ and for a medium length of $L=1$. (b) Sign of the function $G(K, \alpha_0)$. The blue (dark gray) and red (light gray) regions correspond respectively to the negative and positive values of G. The green dots are associated to couples (K, α_0) computed from spatiotemporal numerical simulations for ϕ_L^p varying from 0 to 2π by step of 0.1 ($S_0 = J_0 = 1$).

parameters K and α_0 are limited by the constraints

$$K \in [\max(I_L^s - S_0, I_0^p - J_0), \ \min(I_L^s + S_0, I_0^p + J_0)],$$

$$\alpha_0 \in [0, 2\pi]. \tag{19a}$$

Since H is given by

$$H(z) = H(z = 0) = c(I_0^s, K)\cos(\alpha_0) - d(I_0^s, K), \tag{20}$$

each couple (K, α_0) determines a point (K, H) of the bifurcation diagram. The set of couples (K, α_0) that are solutions of Eq. (18) will be denoted $\{(K, \alpha_0)\}_{sol}$. The question is then to know if $\forall \phi_L^p \in [0, 2\pi]$, there exists at least a couple $(K, \alpha_0) \in \{(K, \alpha_0)\}_{sol}$.

2. Numerical results

Figures 4 and 5 depict two examples of solutions for two different lengths of the nonlinear medium. In Fig. 4, the function G has a line of zero values in the plane (K, α_0) leading to an infinite number of solutions satisfying the
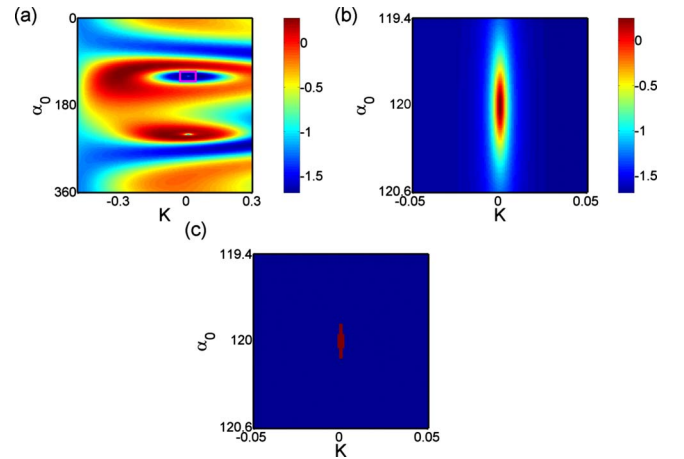
FIG. 5. (Color online) (a) Function $G(K, \alpha_0)$ for the boundary conditions $I_0^s = 0.5$ and $I_L^p = -0.71$ and for a medium length of $L=4$. (b) Zoom of the small part in violet of (a). (c) Sign of the function $G(K, \alpha_0)$ for the values of (b). The blue (dark gray) and red (light gray) regions correspond respectively to the negative and positive values ($S_0 = J_0 = 1$).

boundary conditions on the action coordinates. The set $\{(K,\alpha_0)\}_{sol}$ has a shape that resembles an ellipse around the point of coordinates $(K=0,\ \alpha=2\pi/3)$ [see Fig. 4(b)]. This point corresponds to the doubly pinched torus of the bifurcation diagram since the powers of the two waves are equal. If the angle ϕ_L^p is fixed then there exists a unique possible stationary solution associated to a point of $\{(K,\alpha_0)\}_{sol}$.

For a larger length L, the structure of the function G becomes more complicated, as illustrated in Fig. 5. In particular, we observe new zeros of the function G, which correspond to new possible stationary solutions of the spatiotemporal dynamics. In a neighborhood of the point $(K=0,\ \alpha=2\pi/3)$, we observe the same ellipselike curve which can be obtained by continuity from the preceding ellipse by varying the length L.

This numerical study allows us to propose the following conjecture: there exists in the plane (K,α_0) a closed curve $\mathcal{C}$ around the point $(K=0,\ \alpha=2\pi/3)$ such that for fixed boundary conditions on I_0^s, I_0^p, and ϕ_0^s, each point of $\mathcal{C}$ corresponds to a unique value of ϕ_L^p. We can define a continuous and bijective map from $\mathcal{C}$ to S^1. When the length L increases, the curve $\mathcal{C}$ gets closer to the point $(K=0,\ \alpha=2\pi/3)$, regardless of the boundary conditions. This means that the dynamics lies in a torus very close to the singular torus. It is only in the limit of an infinite length L, that the stationary solution reaches the singular pinched torus. This conclusion is confirmed by the numerical simulations of the PDE system [Eq. (2)], a feature that will be discussed in the next section.

IV. DYNAMICS OF SPATIOTEMPORAL EQUATIONS

In this Section we present numerical simulations of the PDE system [Eq. (2)]. As discussed above in Sec. II, due to the counterpropagating nature of the interaction, boundary conditions are imposed at both ends of the nonlinear medium. Different time-dependent boundary conditions can be considered, depending on the choice of the functions f_1 and f_2. In particular, we introduce here the adiabatic regime in which the boundary conditions are changed slowly from 0 at time $t=0$ toward their asymptotic stationary values.

We shall see that in the adiabatic regime, the spatiotemporal dynamics follows adiabatically the stationary state associated to the singular torus. This feature is consistent with the results of the previous Section, namely that in the limit of a short length L, there exists a unique stationary solution compatible with the boundary conditions and that such solution lies in the vicinity of the singular torus. Furthermore, the numerical simulations of the PDE system [Eq. (2)] reveal that the stationary state converges exponentially toward the singular torus as the length L of the medium increases.

A. Principles of the adiabatically varying boundary conditions

The idea of the adiabatic approach discussed here is twofold. (i) It allows us to consider boundary conditions that are realistic from an experimental point of view. As explained in Sec. II, when a wave is injected in a medium, its amplitude varies progressively from 0 to its stationary value. In the adiabatic approach, such a variation of the boundary condi-
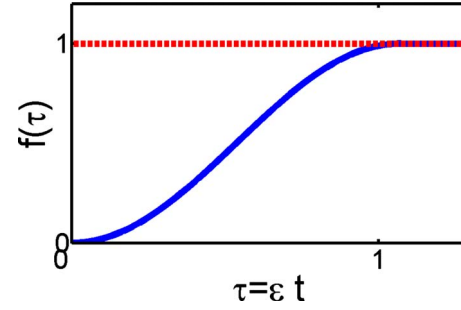
FIG. 6. (Color online) Plot of the function f in blue (dark gray) as a function of τ that has been used in the numerical simulations.

tion is supposed to be slow. (ii) The adiabatically varying boundary conditions also avoid the emergence of spatiotemporal instabilities or singularities in the field amplitudes, a dynamical feature that we have observed in the numerical simulations when the boundary conditions exhibit abrupt variations.

The space-time variation of the boundary conditions is given as follows. First of all, we assume that at time $t=0$ the field in the nonlinear medium is zero,

$$\begin{cases} \vec{S}(z,t=0) = \vec{0}, & \forall z \in [0,L] \\ \vec{J}(z,t=0) = \vec{0}, & \forall z \in [0,L]. \end{cases} \quad (21)$$

Next, let us denote by $(S_0^f)^2$ and $(J_0^f)^2=1$ the respective values of the asymptotic powers of the signal and pump waves (note that due to the adopted normalization $J_0^f=1$). At these powers we associate the final boundary conditions $\vec{S}_f = (S_x^f, S_y^f, S_z^f)$ and $\vec{J}_f = (J_x^f, J_y^f, J_z^f)$. The time-dependent boundary conditions may thus be written as

$$\begin{cases} \vec{S}(z=0,\tau) = f(\tau)\vec{S}_f \\ \vec{J}(z=L,\tau) = f(\tau)\vec{J}_f, \end{cases} \quad (22)$$

where $f=f_1=f_2$ is a smooth monotonic function with values in the interval [0, 1]. The parameter defined by $\tau=\varepsilon t$ with $\varepsilon \ll 1$ is the temporal parameter associated to the adiabatic character of the method. Figure 6 represents the following example of function f,

$$f(\tau) = \begin{cases} \sin^2\left(\dfrac{\pi}{2T}t\right) = \sin^2\left(\dfrac{\pi}{2}\tau\right) & \text{for } \tau \in [0,1] \\ 1 & \text{for } \tau > 1 \end{cases} \quad (23)$$

This function has been used in the numerical simulations in this section. $T=1/\varepsilon$ is the time needed for the field to reach its final value at the incoming boundary. Here we assumed that the time variation of the two waves is the same, but their amplitudes and powers can be different. The generalization to different functions $f_1 \neq f_2$, where the two fields are injected at different times, will be discussed in Sec. IV C. We underline that with this adiabatic treatment of the boundary conditions we have not observed the emergence of instabilities, even for very long lengths L of the nonlinear medium (see Fig. 7).

The numerical simulations of the PDE system [Eq. (2)] reveal that, as a general rule, the spatiotemporal dynamics
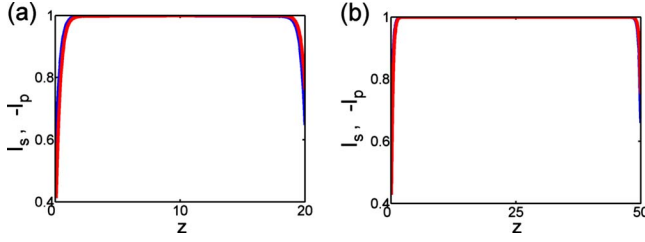
FIG. 7. (Color online) Signal and pump stationary states in the adiabatic approach. The lengths are $L=20$ (a) and $L=50$ (b). The boundary conditions are $I_0^s=0.5$, $\phi_0^s=\pi/4$, $I_L^p=-0.71$ and $\phi_L^p=\pi$. The blue (dark gray) and red (light gray) curves represent respectively the signal and the pump.

follows adiabatically the stationary state associated to the boundary conditions $\vec{S}(0,t)$ and $\vec{J}(L,t)$. In order to explain this observation, we adapt the adiabatic theory developed in classical and quantum mechanics [16] to the spatiotemporal wave system considered here. To avoid cumbersome notations, the following vector will be used to denote both the forward and backward waves:

$$\underline{S} = (\vec{S}, \vec{J}). \tag{24}$$

The nonlinear propagation Eqs. (2) can be written in the general form

$$\frac{\partial \underline{S}}{\partial t} \pm \frac{\partial \underline{S}}{\partial z} = \underline{P_2}(\underline{S}, \underline{S}^*), \tag{25}$$

where $\underline{P_2}(\underline{S}, \underline{S}^*)$ are polynomials of order 2 in $\underline{S}$ and $\underline{S}^*$. The change of variables

$$\underline{S} = f(\tau)\underline{\mathcal{S}} \tag{26}$$

leads to a nonautonomous evolution equation whose advantage relies on the fact that the boundary conditions no longer depend on t,
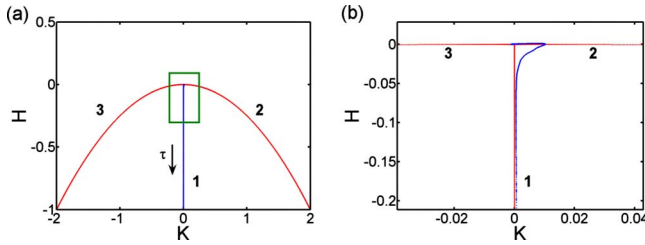
FIG. 8. (Color online) (a) Evolution of the positions of singular tori obtained by the theory in red (light gray) and corresponding evolution of the constants of motion obtained by solving numerically the PDE system [Eq. (2)] in blue (dark gray). The line (1) corresponds to the evolution of the double pinched torus while lines (2) and (3) are associated to critical fibers belonging to the boundary of the bifurcation diagram. The black arrow indicates the direction of the evolution. (b) Zoom of the green panel in (a): the spacetime dynamics of the PDE system [Eq. (2)] follows adiabatically the singular pinched torus. The boundary conditions are $I_0^s=0.5$, $\phi_0^s=\pi/4$, $I_L^p=-0.71$, and $\phi_L^p=\pi$. The length of the medium is $L=20$.

$$\varepsilon \frac{\partial f(\tau)}{\partial \tau}\underline{\mathcal{S}} + f(\tau)\left[\varepsilon \frac{\partial \underline{\mathcal{S}}}{\partial \tau} \pm \frac{\partial \underline{\mathcal{S}}}{\partial z}\right] = |f(\tau)|^2 \underline{P_2}(\underline{\mathcal{S}}, \underline{\mathcal{S}}^*). \tag{27}$$

We are looking for solutions of Eq. (27) in the interval $t \in [0, T]$ in the limit $\varepsilon \to 0$. As in a standard adiabatic theory, we consider a polynomial expansion in the small parameter ε. We write the solution as a sum of terms

$$\underline{\mathcal{S}}(z, \tau) = \underline{\mathcal{S}}^{(0)}(z, \tau) + \varepsilon \underline{\mathcal{S}}^{(1)}(z, \tau) + \varepsilon^2 \underline{\mathcal{S}}^{(2)}(z, \tau)$$
$$+ \cdots + \varepsilon^k \underline{\mathcal{S}}^{(k)}(z, \tau) + \mathcal{O}(\varepsilon^k). \tag{28}$$

We obtain the equations for $\underline{\mathcal{S}}^{(k)}$ by inserting Eq. (28) into Eq. (27) and by identifying the terms with the same order in ε. For instance, we have for the order 0,

$$\varepsilon^0: \pm f(\tau)\frac{\partial \underline{\mathcal{S}}^{(0)}}{\partial z} = |f(\tau)|^2 \underline{P_2}(\underline{\mathcal{S}}^{(0)}, \underline{\mathcal{S}}^{(0)*}), \tag{29}$$

and for the order 1,

$$\varepsilon^1: \varepsilon \frac{\partial f(\tau)}{\partial \tau}\underline{\mathcal{S}}^{(0)} + f(\tau)\left[\varepsilon \frac{\partial \underline{\mathcal{S}}^{(0)}}{\partial \tau} \pm \frac{\partial \underline{\mathcal{S}}^{(1)}}{\partial z}\right] = |f(\tau)|^2 \underline{P_2^1}(\underline{\mathcal{S}}^{(0)}, \underline{\mathcal{S}}^{(1)}), \tag{30}$$

where $\underline{P_2^1}(\underline{\mathcal{S}}^{(0)}, \underline{\mathcal{S}}^{(1)})$ is a polynomial of order 2, each term being the product of a term of the form $\underline{\mathcal{S}}^{(0)}$ and a term of the form $\underline{\mathcal{S}}^{(1)}$.

From Eq. (29), we can conclude that the term of order 0, $\underline{\mathcal{S}}^{(0)}(z, \tau)$, is an instantaneous stationary solution corresponding to a given value of τ. For ε small enough, the spatiotemporal dynamics will then follow continuously the stationary state associated to the boundary conditions at time τ.

B. Adiabatic evolution of the system and exponential convergence to the singular torus

Let us now recall an important result established in the previous Sec. III C, namely, that for small lengths of the nonlinear medium $(L \to 0)$ there exists a unique stationary solution compatible with the boundary conditions, and that such a stationary solution is close to the singular torus. Note that, according to the normalization adopted in this work, the length L is normalized to Λ_0, so that a small length L also means a small power of the beams. Now one should consider that, at the beginning of the interaction (i.e., when the beams enter the medium), the powers of the beams are small since their values increase from zero. This implies that the two waves follow the stationary solution associated to the singular torus at the beginning of the interaction, since this solution is the unique available stationary solution. As the beams progressively enter the medium, their powers increase and new stationary solutions compatible with the boundary conditions emerge (see Sec. III C). However, because the boundary conditions are slowly varying, the system adiabatically follows the initial stationary solution, i.e., the stationary solution associated to the singular torus. In this way, the system remains close to the solution in the neighborhood of the singular torus during its whole evolution.

This conclusion is confirmed by the numerical simulations of the PDE system [Eq. (1)], as illustrated in Fig. 8. For
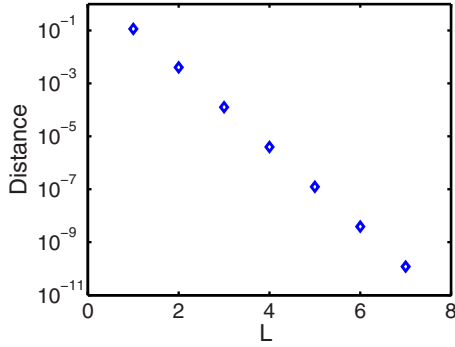
FIG. 9. (Color online) Evolution of the distance in the phase-space diagram $\rho = \sqrt{H^2 + K^2}$ between the singular torus and the regular torus on which lies the stationary state for a given length L: the stationary state converges exponentially toward the singular torus.

every time τ, we determine the position $[K^f(\tau), H^f(\tau)]$ of the singular tori in the bifurcation diagram. We then compute from spatiotemporal dynamics, the point $[K_{sp}(\tau), H_{sp}(\tau)]$, defined by the following relations at time τ:

$$K_{sp}(\tau) = \frac{1}{L} \int_0^L K(\tau) dz, \tag{31a}$$

$$H_{sp}(\tau) = \frac{1}{L} \int_0^L H(\tau) dz. \tag{31b}$$

We see in Fig. 8 that, as expected, the curve defined by $[K_{sp}(\tau), H_{sp}(\tau)]$ follows continuously the curve defined by $[K^f(\tau), H^f(\tau)]$, thus confirming that the spatiotemporal PDE dynamics follows adiabatically the position of the singular pinched torus.

As discussed above, for a finite length L of the nonlinear medium, the relaxation process does not occur exactly *on* the singular torus, but in the neighborhood of it [26]. Actually, the numerical simulations reveal that the stationary state *converges exponentially* toward the pinched torus in the limit of an infinite length, $L \to +\infty$. This result is illustrated in Fig. 9, that reports the distance to the singular torus as a function of the length of the nonlinear medium L. This figure has been obtained by performing numerical simulations of the PDE system [Eq. (2)] for different values of L. Once the stationary state was reached, we calculated the euclidian distance ρ between the singular torus and the regular torus associated to the stationary solution. Such a distance has been calculated in the phase-space diagram, $\rho = \sqrt{H^2 + K^2}$. Figure 9 shows that the convergence toward the singular torus exhibits an exponential law, a feature which is confirmed over more than ten orders of magnitude. We conjecture that the origin of the exponential behavior lies on the logarithmic divergence of one of the periods of the torus as the distance between this torus and the pinched torus tends to zero.

C. Nonsimultaneous injection of initial impulsions

Up to now, we have considered the case where the waves are simultaneously injected into the medium. However, from the experimental point of view, it could be more realistic to
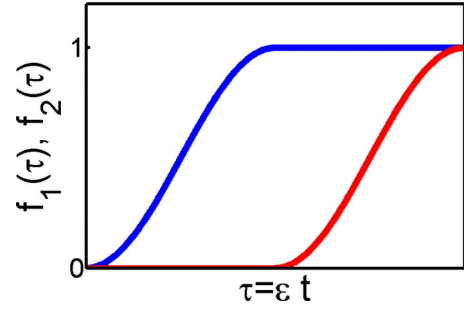
FIG. 10. (Color online) Functions f_1 in blue (dark gray) and f_2 in red (light gray) as a function of τ which are used in the study of the nonsimultaneous injection of the waves. The pump corresponding to f_1 is injected before the signal wave corresponding to f_2.

consider a nonsimultaneous injection of the pump and the signal waves. In this Section we analyze this problem by considering the case where the pump wave is injected before the signal wave. The corresponding boundary conditions read

$$\begin{cases} \vec{J}(z = L, t) = f_1(\tau) \vec{J}_f, \\ \vec{S}(z = 0, t) = f_2(\tau) \vec{S}_f \end{cases} \tag{32}$$

where $f_1(\tau)$ and $f_2(\tau)$ are displayed in Fig. 10.

As opposed to the case analyzed above in which the two waves are injected simultaneously, here the ratio of the powers S_0^2 / J_0^2 is not constant during the time evolution. This leads to a different spatiotemporal dynamics of the system. This aspect is shown in Fig. 11. We underline that the bifurcation diagram and thus the temporal evolutions of singular tori depend on the ratio S_0 / J_0. During the injection of the signal, for small values of S_0, the bifurcation diagram does not exhibit pinched tori. We observe in the simulations of the PDE system [Eq. (2)] that the spatiotemporal dynamics relaxes toward an oscillatory stationary state, as illustrated in Fig. 11(b). For larger values of S_0, pinched singular tori emerge in the bifurcation diagram, as can be verified in Fig. 11(a) for $H < -0.5$. The spatiotemporal dynamics then jumps into the stationary state associated to the pinched torus. This is displayed in Fig. 11(a), which shows that, whenever the PDE dynamics has a pinched torus, it then follows adiabatically its temporal evolution, as confirmed by the superposition of the red and blue lines. We also report in Fig. 11(c) the corresponding stationary state obtained by the numerical simulations, which is the stationary state associated to the pinched torus located near $H \simeq -1$, $K \simeq 0$ in the bifurcation diagram [Fig. 11(a)].

In this Section we have thus shown that in the framework of the adiabatic approach, singular tori play a major role not only for the determination of the asymptotic stationary state, but also for the spatiotemporal dynamics of the four-wave system.

V. CONCLUSION AND PERSPECTIVES

In summary, we have discussed the role of singular tori in the spatiotemporal dynamics of the four-wave interaction in
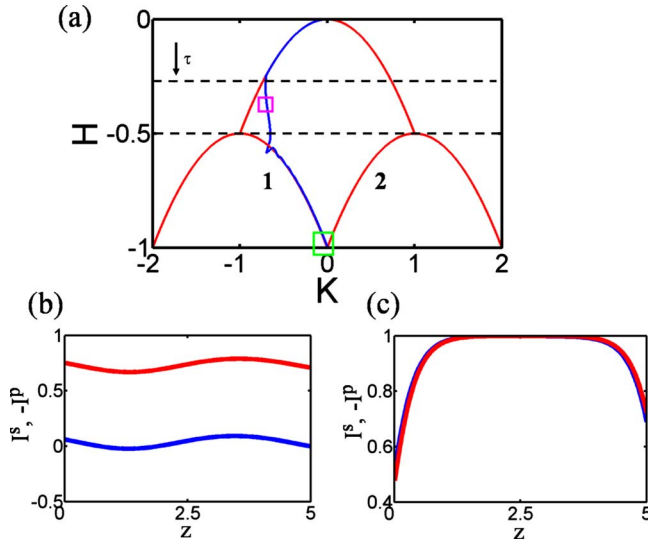
FIG. 11. (Color online) (a) Evolution of the positions of singular tori in red (light gray) and of the point of coordinates (K_{sp}, H_{sp}) in blue (dark gray). The lines (1) et (2) correspond to the evolution of the pinched tori. The black arrow indicates the time evolution. The time interval between the two dashed lines corresponds to the injection of the signal wave. (b) Stationary state associated to the region in the pink square (upper square) on (a). (c) Stationary state associated to the region in the green square (lower square) on (a). The (final) boundary conditions are $I_0^s = 0.5$, $\phi_0^s = \pi/4$, $I_L^p = -0.71$ et $\phi_L^p = \pi$. The length of the nonlinear medium is $L = 5$.

its counterpropagating configuration. An adiabatic approach reveals that for slowly varying boundary conditions, the spatiotemporal dynamics follows adiabatically the stationary state corresponding to the singular torus of the associated bifurcation diagram. In this sense, singular tori appear as attractors for the spatiotemporal dynamics of the four-wave interaction. Furthermore, as discussed in Ref. [26], singular tori also play a major role in the resonant three-wave interaction or in the dynamics of wave propagation in periodic media, which find applications in optics, hydrodynamics, plasmas, or condensed matter physics. Our preliminary work shows that the adiabatic theory developed here for the four-wave interaction may be easily extended to the spatiotemporal dynamics of the three-wave interaction or to nonlinear wave dynamics in periodic systems.

As discussed in detail in Refs. [27,28], besides its fundamental interest, the attraction process discussed here may be exploited to achieve complete polarization of unpolarized light [15]. Indeed, in contrast to standard polarizers that unavoidably waste 50% of unpolarized light, here the repolarization process may take place, in principle, with 100% efficiency, i.e., without any loss of energy[27,28].

Another open question is the extension of these results to PDE systems whose associated stationary Hamiltonian is not integrable. In this case, the Hamiltonian dynamics of the stationary states belongs to a mixed regime of regular and chaotic trajectories, which is known to be described by the Kolmogorov-Arnold-Moser theorem. For sufficiently small nonintegrable perturbations, rational tori are destroyed but irrational tori are preserved or transformed into cantori. The singular tori become stable and unstable manifolds of hyperbolic orbits, with generically transverse intersections. For larger nonintegrable perturbations, an increasing portion of the phase space is invaded by chaotic trajectories [29]. Considering that Hamiltonian monodromy is a topological property related to the presence of singular pinched tori [17], this concept can still be defined for Hamiltonian systems sufficiently close to integrable ones [31,30]. Accordingly, we may expect that the phenomenon of relaxation discussed in this paper should persist in the presence of small nonintegrable perturbations. Work is in progress to study this problem.

[1] R. Z. Sagdeev, D. A. Usikov, and G. M. Zaslavsky, *Nonlinear Physics* (Harwood Academy Publishers, Chur, 1988).

[2] J. Weiland and H. Wilhelmsson, *Coherent Nonlinear Interaction of Waves in Plasmas* (Pergamon, Oxford, 1977).

[3] M. F. Hamilton and D. T. Blackstock, *Nonlinear Acoustics* (Academic Press, New York, 1998).

[4] E. Infeld and G. Rowlands, *Nonlinear Waves, Solitons and Chaos* (Cambridge University Press, Cambridge, England, 1992).

[5] R. W. Boyd, *Nonlinear Optics*, 3rd ed. (Academic Press, New York, 2008).

[6] L. Deng *et al.*, Nature (London) **398**, 218 (1999).

[7] J. Heurich, H. Pu, M. G. Moore, and P. Meystre, Phys. Rev. A **63**, 033605 (2001).

[8] S. Inouye *et al.*, Science **285**, 571 (1999); Nature (London) **402**, 641 (1999).

[9] G. P. Agrawal, *Nonlinear Fiber Optics*, 4th ed. (Academic, New York, 2006).

[10] D. J. Gauthier, M. S. Malcuit, A. L. Gaeta, and R. W. Boyd, Phys. Rev. Lett. **64**, 1721 (1990).

[11] G. Gregori and S. Wabnitz, Phys. Rev. Lett. **56**, 600 (1986); A. L. Gaeta, R. W. Boyd, J. R. Ackerhalt, and P. W. Milonni, *ibid.* **58**, 2432 (1987); A. L. Gaeta and R. W. Boyd, Phys. Rev. A **48**, 1610 (1993).

[12] J. Yumoto and K. Otsuka, Phys. Rev. Lett. **54**, 1806 (1985); S. Trillo and S. Wabnitz, Phys. Rev. A **36**, 3881 (1987); M. V. Tratnik and J. E. Sipe, *ibid.* **35**, 2976 (1987); **36**, 4817 (1987); D. J. Gauthier, M. S. Malcuit, and R. W. Boyd, Phys. Rev. Lett. **61**, 1827 (1988).

[13] D. David, D. D. Holm, and M. V. Tratnik, Phys. Rep. **187**, 281 (1990).

[14] S. Pitois, G. Millot, and S. Wabnitz, J. Opt. Soc. Am. B **18**, 432 (2001); Phys. Rev. Lett. **81**, 1409 (1998).

[15] S. Pitois, A. Picozzi, G. Millot, H. R. Jauslin, and M. Haelterman, Europhys. Lett. **70**, 88 (2005); S. Pitois, J. Fatome, and G. Millot, Opt. Express **16**, 6646 (2008).

[16] V. I. Arnol'd, *Mathematical Methods of Classical Mechanics* (Springer-Verlag, New York, 1989).

[17] R. H. Cushman and L. Bates, *Global Aspects of Classical Integrable Systems* (Birkhauser, Basel, 1997).

[18] K. Efstathiou, *Metamorphoses of Hamiltonian Systems with Symmetry*, Lecture Notes in Mathematics (Springer-Verlag, Heidelberg, 2004).

[19] A. V. Bolsinov and A. T. Fomenko, *Integrable Hamiltonian Systems: Geometry, Topology, Classification* (Chapman and Hall, CRC, Boca Raton, 2004).

[20] D. Sugny, P. Mardešić, M. Pelletier, A. Jebrane, and H. R. Jauslin, J. Math. Phys. **49**, 042701 (2008).

[21] J. J. Duistermaat, Commun. Pure Appl. Math. **33**, 687 (1980).

[22] R. H. Cushman, H. R. Dullin, A. Giacobbe, D. D. Holm, M. Joyeux, P. Lynch, D. A. Sadovskií, and B. I. Zhilinskií, Phys. Rev. Lett. **93**, 024302 (2004).

[23] K. Efstathiou, O. V. Lukina, and D. A. Sadovskií, Phys. Rev. Lett. **101**, 253003 (2008).

[24] H. R. Dullin and H. Waalkens, Phys. Rev. Lett. **101**, 070405 (2008).

[25] D. A. Sadovskií and B. I. Zhilinskií, Phys. Lett. A **256**, 235 (1999).

[26] D. Sugny, A. Picozzi, S. Lagrange, and H. R. Jauslin, Phys. Rev. Lett. **103**, 034102 (2009).

[27] J. E. Heebner, R. Bennink, R. W. Boyd, and R. Fischer, Opt. Lett. **25**, 257 (2000).

[28] A. Picozzi, Opt. Express **16**, 17171 (2008).

[29] M. Tabor, *Chaos and Integrability in Nonlinear Dynamics* (Wiley, New York, 1989).

[30] B. W. Rink, Nonlinearity **17**, 347 (2004).

[31] H. Broer, R. Cushman, F. Fasso, and F. Takens, Ergod. Theory Dyn. Syst. **27**, 725 (2007).